Cement and Concrete Research 39 (2009) 849–860

Contents lists available at ScienceDirect

Cement and Concrete Research

journal homepage: http://ees.elsevier.com/CEMCON/default.asp

# Studying nucleation and growth kinetics of alite hydration using μic

Shashank Bishnoi *, Karen L. Scrivener

*Ecole Polytechnique Fédérale de Lausanne, EPFL-STI-IMX-LMC, Station 12, 1015 Lausanne, Switzerland*

ARTICLE INFO

*Article history:*
Received 6 February 2009
Accepted 3 July 2009

*Keywords:*
Alite
Hydration
Kinetics
Modelling
Microstructure
Calcium–silicate–hydrate (C–S–H)

ABSTRACT

This paper investigates the applicability of nucleation and growth mechanisms to the hydration of alite. Various possible mechanisms of nucleation and growth were simulated using the recently-developed microstructural modelling platform μic. Comparison with the Avrami equation and the boundary nucleation model demonstrate the limitations of these equations. Experimental measurements of the rates of hydration of alite powders with different particle size distributions were then simulated with a boundary nucleation and growth model in μic. The results show that while the nucleation and growth of C–S–H having bulk densities in the currently accepted range can explain the acceleration during the first few hours of hydration, it cannot explain the later deceleration. It was also found that the resistance to flow of ions offered by the layer of hydrates forming over the surface of the alite particles (diffusion control) cannot explain the deceleration. The deceleration could be reproduced when C–S–H was assumed to be loosely packed in the beginning with its density of packing increasing with hydration. It is proposed that during the early hours of hydration a loosely-packed C–S–H fills a large fraction of the microstructure and the further development of its microstructure occurs due to an increase in its packing.



## 1. Hydration kinetics of alite

This paper investigates the hydration kinetics and mechanisms of alite during the first day or so of hydration. Alite is an impure form of tri-calcium silicate ($3CaO.SiO_2$, simply called $C_3S$ by cement chemists) and is the main phase in Portland cements. Its hydration is the major contributor to the most important properties of hardened cement paste such as strength and durability. This is especially true during the first few days of hydration, during which a large amount of C–S–H, the most important hydration product, forms by the hydration of alite. Although other phases such as aluminates also play an important role in the development of these properties, the simultaneous hydration of several phases in cement makes experimental results difficult to interpret and quantitative kinetics studies difficult for cement as a whole. For this reason, the current study focuses on the hydration of alite in a single phase system.

The hydration kinetics of alite are similar to those of Portland cement. The main stages of activity exhibited by alite in isothermal calorimetry measurements are identified below.

1. The dissolution period: during the first period, high activity attributed to the rapid dissolution of alite in water is observed.
2. The induction period: during the following hour or so low activity is observed.
3. The acceleration period: the rate of hydration increases dramatically for several hours.
4. The deceleration period: the rate of hydration reduces to much lower levels.
5. Slow hydration period: after the decelerating period, the hydration rates settle to much lower and slowly reducing values.

This study focuses on the third and fourth stages of hydration (acceleration and deceleration), during which the mechanism of nucleation and growth is assumed to predominate [1–4].

### 1.1. Nucleation and growth mechanisms in alite hydration

A nucleation and growth mechanism involves the formation of small nuclei of a phase and their continuous growth at a rate proportional to the free area of the nuclei. The increasing surface area of the nuclei leads to an increase in the rate of the reaction, but eventually impingement of the products leads to a reduction in the rate of reaction. It is assumed that the availability of the converting materials and their transport to the growth sites do not control the rate of conversion. In the case of alite, it is generally accepted that small nuclei of C–S–H form on the surface of alite particles a few minutes after alite is brought in contact with water, and it is the growth of this product that controls the hydration kinetics in stage 3 [3,4]. While it has often been argued that the slow diffusion of ions through the layers of hydrates depositing over the alite particles leads to the deceleration in stage 4 [5–7], it has been shown that nucleation and growth mechanism can also explain the deceleration observed in stage 4 [4]. The saturated bulk density of this product is thought to vary between 1.9 and 2.1 g/cm$^3$ [8].

* Corresponding author.
*E-mail address:* shashank.bishnoi@gmail.com (S. Bishnoi).

0008-8846/$ – see front matter © 2009 Elsevier Ltd. All rights reserved.
doi:10.1016/j.cemconres.2009.07.004

The Avrami equation [9–11], which models the nucleation and growth of nuclei randomly distributed in a solidifying melt and was originally empirically derived to model the decomposition of austenite [12], has been widely used to model alite and cement hydration [1–3,13]. A commonly used form of the relation is shown in Eq. (1).

$$f = 1 - \exp(-k_1 \cdot t^n) \tag{1}$$

In this equation, $k_1$ is a rate constant and $f$ is the fraction of material reacted as a function of time, $t$. The parameter $n$ can further be defined as:

$$n = P + Q \tag{2}$$

where $P$ is the dimensionality of growth of products and $Q$ is 1 for systems with a constant nucleation rate throughout the reaction and 0 for cases where only an initial nucleation event occurs [14].

The use of the Avrami equation for cements has been criticised since the nucleation is not completely random and usually limited to the surface of alite particles [3,4]. It has been shown that a slightly modified form of the boundary nucleation (BN) model, which was developed by Cahn [15] for systems where the nuclei form at a constant rate on randomly distributed boundaries and grow at a constant rate, can be used to reproduce both the acceleration and deceleration in alite hydration [4]. In the BN model, the fraction of volume converted at any moment in time can be calculated using Eq. (3), where $S$ is the nucleation surface available per unit volume, $I$ is the number of nuclei formed per unit unconverted surface per unit time, $G$ is the rate of growth of individual nuclei and $y$ is a dummy variable.

$$f = 1 - \exp\left[S \cdot \int_0^{G \cdot t} \left[1 - \exp\left(-\pi \cdot I\left(\frac{G^2 \cdot t^3}{3} + \frac{2y^3}{3G} - y^2 \cdot t\right)\right)\right] dy\right] \tag{3}$$

The derivation of both the Avrami and BN equations first involves calculating the extended volume fraction ($V^*$) of the growing material, which is the volume that would have been occupied neglecting the overlaps between particles. The real volume of the material ($V$) is then calculated assuming:

$$\frac{dV}{dt} = (1 - V)\frac{dV^*}{dt} \Rightarrow V = 1 - \exp(-V^*) \tag{4}$$

The above assumption, while valid in many cases, is only an approximate way of accounting for the overlaps between particles and may not be applicable to certain systems.

The applicability of the Avrami and BN equations to alite like systems is investigated in this paper using the microstructural modelling platform μic [16,17]. μic is an open-source three-dimensional microstructural modelling platform that allows users to define their problem in terms of customised materials and reactions. Users of μic can also define models of various mechanisms such as hydration kinetics, growth mechanisms, variation in density, rates and locations of nucleation, etc. using plugins. Since μic treats each particle individually, the varied distribution of particle sizes is automatically taken into account. Furthermore, since the potential overlaps between all particles are explicitly calculated in μic, assumptions such as that in Eq. (4) are not required. More information about the μic platform and plugins can be found elsewhere [16,17].

A deeper investigation of different possible hydration mechanisms, including two variations of nucleation and growth mechanisms and a diffusion controlled mechanism was then carried out. A comparison of experimental results from Costoya [18] with simulations of the mechanisms in μic show that neither of the currently accepted nucleation and growth mechanism, nor a diffusion controlled mechanism can explain the deceleration in stage 4 of hydration. A new hypothesis that can explain this deceleration is proposed.

## 2. Simulating homogeneous and boundary nucleation and growth

### 2.1. Homogeneous nucleation

Two simulations, A and B, were carried out to study the reaction rate in a system with homogeneous (random) nucleation and growth, similar to the scenario studied by Avrami [10]. In these simulations, randomly dispersed spherical nuclei grow at a rate proportional to their individual free surface area. As the nuclei grow their free surface increases, then impingement with neighbouring nuclei leads to a reduction in the free surface. While the Avrami equation accounts for the impingements using the assumption in Eq. (4), all impingements are explicitly calculated in μic. In the first simulation (A) the nuclei were created at a linear rate throughout the simulation ($Q = 1$). In the second simulation (B), all the nuclei were present from the beginning of the simulation ($Q = 0$). Table 1 lists the initial number of nuclei per unit volume ($N_0$), the number of new particles created per unit time per unit volume ($I$) and the increase in radius per unit time for individual particles ($G$) using arbitrary but consistent length and time units. Cubic computational volumes with 100 unit lengths side and periodic boundary conditions were used for the simulations.

Fig. 1 shows snapshots of slices from the simulations. In Fig. 2 the simulated converted volume fraction is plotted against time. The figure also shows the converted volume fraction calculated from the Avrami equation with the parameters used in the simulations (Table 1). The parameter $n$ is calculated based on Eq. (2) above and in three dimensions, the parameter $k_1$ can be calculated using Eq. (5) below.

$$k_1 = \frac{\pi \cdot G^3}{3}(I + 4 \cdot N_0) \tag{5}$$

The excellent agreement between the simulated values and the Avrami equation demonstrates, not only the applicability of Eq. (4) to such systems, but also that μic operates correctly in such scenarios.

### 2.2. Boundary nucleation

Simulations C and D are similar to simulation A, with the added condition that the nucleation is allowed to occur only on the surface of spherical particles distributed randomly in the volume, making these simulations relatively closer to the mechanism thought to be active in the hydration of alite. The initial amount of this substrate material is around 44.25% of the total volume, which is equivalent to a 0.4 water to cement ratio alite paste. The number of nuclei of the product on each substrate particle increased at a rate proportional to the unreacted area of the particle and the rate of increase of radius of each nucleating particle was kept constant. This scenario is similar to that modelled by Cahn [15], with the exception that here the growth is occurring on randomly distributed spherical particles in place of randomly distributed planes.

A small number of substrate particles (1000) were used to limit the number of nucleating particles to a computationally manageable number. In the first simulation (C), the rate of nucleation was lower and the rate of growth was higher than the second simulation (D). The

**Table 1**
Parameters used in the homogeneous nucleation and growth simulations and for calculation using the Avrami equation (lengths and times are in arbitrary units).

| | $N_0$ | $I$ | $G$ | $k$ | $N$ |
|---|---|---|---|---|---|
| Sim. A | 0 | $10^{-4}$ | 0.05 | $1.31 \times 10^{-8}$ | 4 |
| Sim. B | 100 | 0 | 0.05 | $5.24 \times 10^{-6}$ | 3 |

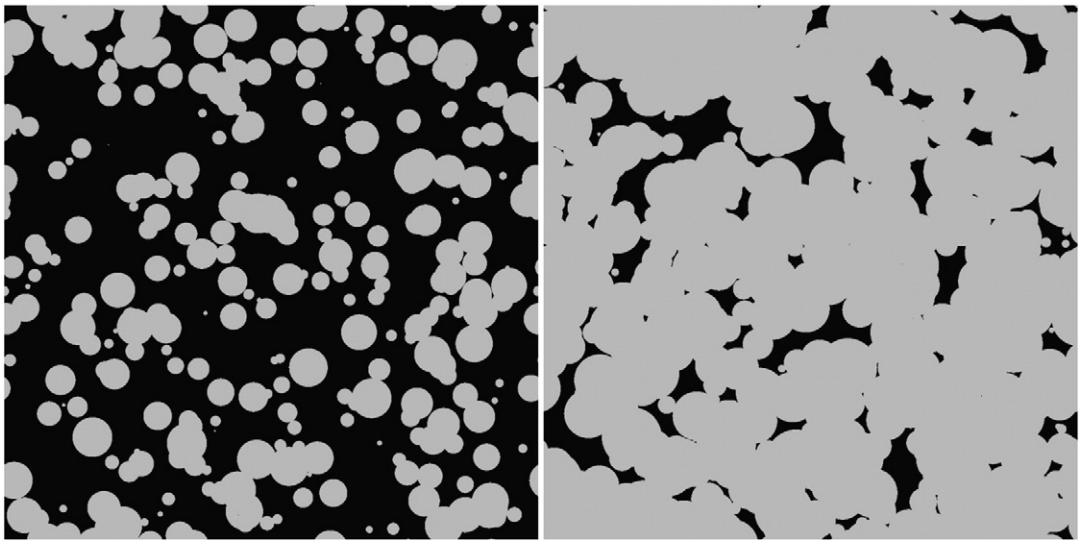

**Fig. 1.** Slices from the first set of simulations, with 36% (left) and 90% (right) of volume filled.

obtained curves were fit with the Avrami (Eq. (1)) and BN (Eq. (3)) equations. The simulated rates of volume conversion and their fits with the Avrami and BN equations are presented in Fig. 3. The parameters used in the simulation and the fit parameters are listed in Table 2. It was seen that although the Avrami equation can be used to fit the early part of the evolution for the two simulations, the fit cannot be extrapolated beyond the acceleration part of the curve and the fit parameters bear no obvious relation to the simulation parameters. This clearly shows that the Avrami equation is not suitable to model systems like alite where nucleation sites are not randomly distributed throughout the volume.

For simulation C, it was possible to obtain an excellent fit with the BN equation by fixing $G$ to the value used in the simulation and freely varying $I$ and $S$. However, the values of $I$ and $S$ obtained do not appear to be related to the simulation parameters. This may be due to the use of spherical substrate particles and the fact that the nucleation density was controlled for each substrate particle. The fits with the BN equation show that once again the assumption in Eq. (4) is valid for these simulations and that μic operates correctly in the scenario modelled by the BN equation.

The deceleration after the peak was found to be much slower in simulation D, compared to simulation C. This is because, at the peak in simulation D, although the impingement between nuclei growing on the same substrate particles is sufficient to stop the acceleration, the impingement between nuclei growing on different substrate particles is not sufficient to lead to a rapid deceleration (see Fig. 4 right). While it was possible to fit the BN equation until just after the peak, the shape of the trend beyond the peak was significantly different.

Simulations C and D show that the validity of Eq. (4), and therefore the Avrami and BN equation, in the scenario modelled depends on the values of the parameters. The potential overlaps between the nuclei depend not only on the overall fraction of volume converted, but also on the distance between the nucleation boundaries. These simulations clearly demonstrate that while the acceleration can be stopped by the impingement between nuclei on the same particle, the deceleration predicted by the BN equation, which resembles the shape observed in stage 4 of alite hydration [4] also requires sufficient impingement between nuclei from different substrate particles.

The possibility of simulating the peak and the deceleration observed in experimentally measured hydration rates of alite with different particle size distributions is studied in the following sections.

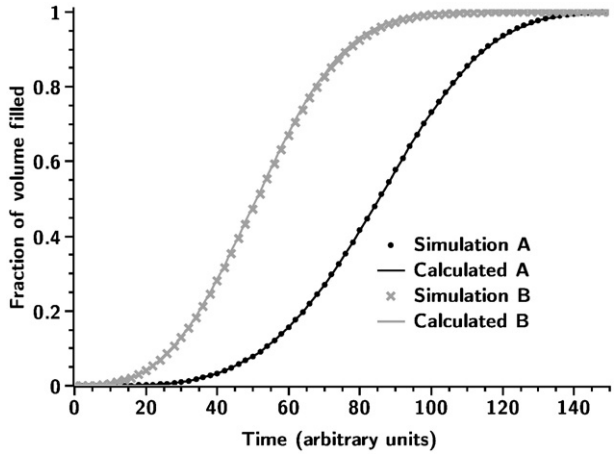


**Fig. 2.** Fit of reaction rates with Avrami equation.

## 3. Study on the effect of particle size distribution on hydration kinetics

The hydration of alite prepared in the laboratory was studied by Costoya [18] by isothermal calorimetry. With this technique, only the total rate of hydration is followed. This rate is a sum of the rates of many particles over a wide range of sizes that may hydrate at different rates. As shown by Knudsen [19], it is difficult to deduce the reaction kinetics at the level of individual particles from overall reaction kinetics, as different rate laws at the particle level may produce very similar overall kinetics at the system level. Therefore, in order to better understand the rate of reaction at the particle level the alite was fractionated into different size ranges of particle using sedimentation. The particle size distributions of the fractions used in this study and the original powder, measured using laser granulometry are shown in Fig. 5.

The particle size distribution (PSD) of the original powder is close to that of cement and the fractions in this study were chosen in order to cover the entire range of particle sizes present in cement. PSD A is the unfractionated powder and the other fractions, B to E, are labelled in order of reducing mode radii. Fractions B, C and D have narrow particle size distributions containing only larger particles and fraction E contains a wider range of particle sizes. Mode details about the fractions are listed in Table 3.

Around 5 g of paste with 0.4 water to cement ratio was used for each sample in the calorimeter. The measured heat-evolution curves per gram of alite are shown in Fig. 6. As expected, the rate of heat

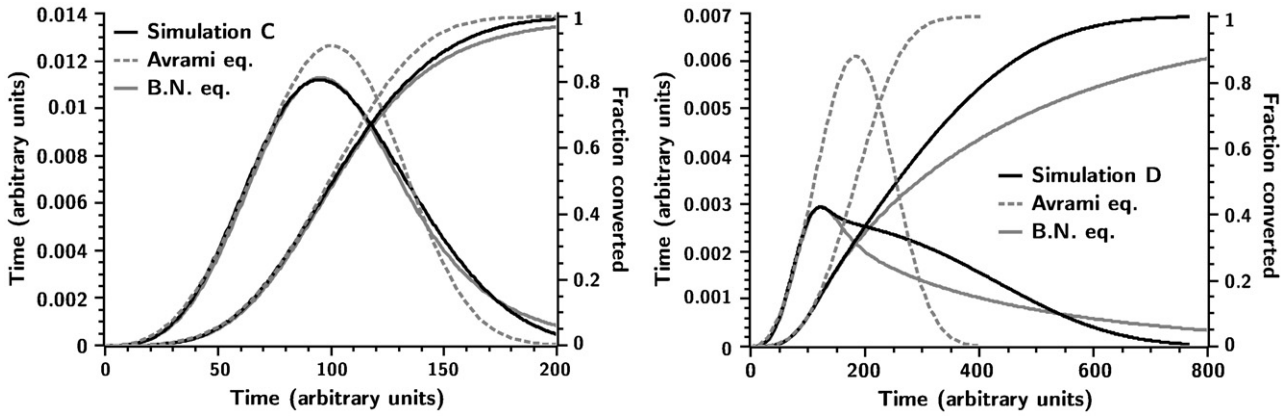


**Fig. 3.** Fits of of the Avrami and BN equation with reaction rates from simulations C (left) and D (right) (see Table 2). The Avrami equation was fit only in the accelerating part of the curve and was extended. The monotonic curves show the fraction converted and the curves with peaks show the rates.

evolution was observed to depend strongly on the particle size distribution, with the finer fractions reacting faster. More details on the experiments can be found in the thesis of Costoya [18]. In the following sub-sections, various possible hydration mechanisms have been investigated using μic on particle size distributions similar to those in the experiments.

### 3.1. Simulating nucleation and growth kinetics for different PSDs of alite

In this set of simulations, the applicability of the traditionally accepted nucleation and growth mechanism to alite hydration, as discussed in Section 1.1, is investigated using μic. Numerical studies of nucleation and growth mechanism in two dimensions [3], have suggested that the rates of reaction observed can be explained by the growth of product over alite particles, with the acceleration period ending when the entire surface becomes covered by the product. However, these simulations were made in two dimensions and the effects of space filling and the presence of other particles is not taken into account. In μic it is possible to model a similar process in three-dimension accounting for all impingements in regions of hydration product originating from different particles. The process of nucleation and growth was simulated on particle size distributions, as measured using laser diffractometry, similar to those used in the experiments discussed earlier. The water to cement ratio was kept at 0.4 for all simulations and the specific heat of hydration of alite was assumed to be 500 kJ/g [20].

The simplifications used in the simulations were:

- The particles were assumed to be spherical and randomly distributed in space,
- The first two stages of hydration (dissolution and induction) have been neglected as the amount of reaction at the end of the second stage is generally quite small,
- The inner product was assumed to completely fill the space created by the dissolving particles, and
- At any moment the same fraction of all particles was assumed to be covered.

It is understood that the effect of the above simplifications on the calculated values may not necessarily be negligible, however, they are not expected to significantly alter the shape of the heat-evolution curves. Furthermore, the simulations only explore whether various mechanisms can explain the observed experimental results and the simulations are not intended to provide perfect fits. It must be noted that, apart from the assumption of spherical particles, the others are not essential in μic and have been used only to simplify the calculations.

In all calculations, μic ensures that:

- Mass is conserved by strictly following the stoichiometry of the defined reactions,
- All space is accounted for in the calculations, such that products grow only at locations that are not already occupied,
- At any moment in time. the size of individual layers of each particle corresponds to the mass and the density of the materials contained in the layer, and
- The available surface for growth on the product is calculated individually for each particle and all possible overlaps are calculated.

The equation for the hydration of alite (Eq. (6)) can be converted to volumetric terms as shown in Eq. (7), assuming a density of 3.15 g/cm$^3$ for alite, 1.0 g/ml for water, 2.0 g/cm$^3$[1] for C–S–H and 2.24 g/cm$^3$ for CH.

$$C_3S + 5.3H \rightarrow C_{1.7}SH_4 + 1.3CH \quad (6)$$

$$1.0 \cdot V_{C_3S} + 1.318 \cdot V_H \rightarrow 1.569 \cdot V_{C-S-H} + 0.593 \cdot V_{CH} \quad (7)$$

In these simulations the C–S–H is assumed to grow on the surface of the alite particles, while the CH is assumed to form new particles in the pores. The CH nuclei were assumed to form at random locations, growing at random rates such that the total growth equals the production of CH from the reaction. Based on the work of Jennings and Parrott [21], and Navi and Pignat [22], the CH particles were assumed to nucleate at an exponentially reducing rate and the final number was fixed at 20% of the number of alite particles in case of fractions

**Table 2**
Details of the boundary nucleation and growth simulations and parameters used to fit Avrami and BN equations to simulations C and D.

| | Simulation | | | | Avrami eq. | | BN eq. | | |
|---|---|---|---|---|---|---|---|---|---|
| | Final number of nuclei | $I$ | $G$ | $S$ | $k_1$ | $n$ | $I$ | $G$ | $S$ |
| Sim. C | 79,795 | 0.005 | 0.02 | 0.43 | $4.04\times10^{-8}$ | 3.62 | 0.00175 | 0.02 | 1.15 |
| Sim. D | 1,643,311 | 0.05 | 0.005 | 0.43 | $3.17\times10^{-8}$ | 3.24 | 0.038 | 0.005 | 0.53 |

[1] This value is commonly assumed for water saturated C–S–H. If a different value were taken this would not have a significant impact on the shape of the curves.

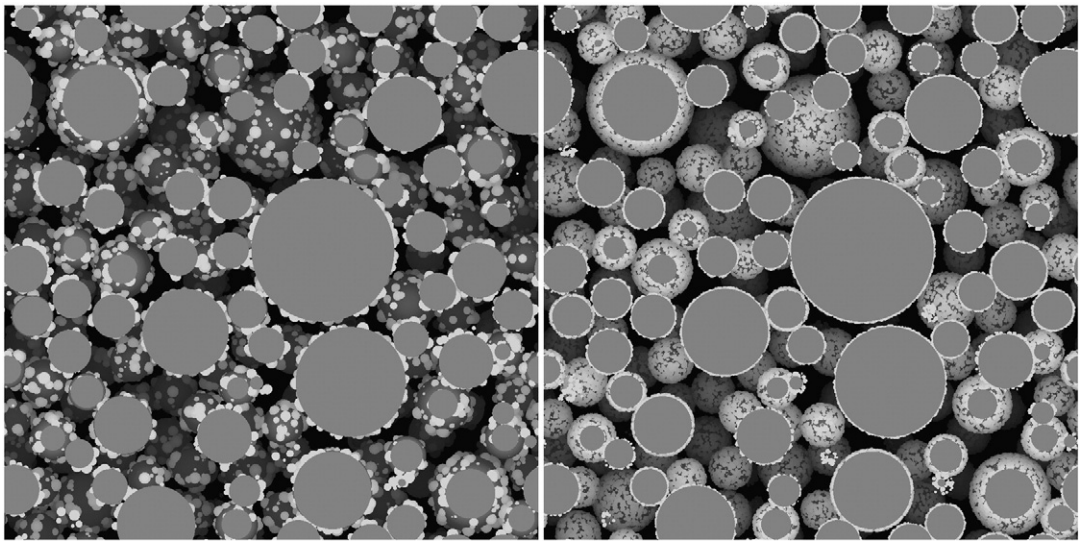

**Fig. 4.** Three-dimensional slices from simulations C (left) and D (right) at around 10% conversion of free volume.

with fine particles and 50% of the number of alite particles for fractions without fine particles. The number and rate of formation of CH particles do not significantly affect the results.

Table 4 lists the number of alite particles resulting from the particle size distribution defined and the size of computational volume used in the simulations for all the fractions. The size of the computational volume was chosen based on the size of the largest particle in the system.

In the simulations the hydration kinetics were assumed to be governed solely by the nucleation and growth of the product on the reacting particles. Small nuclei of C–S–H form at random locations on the surface of the reacting particles. The nuclei grow at a fixed rate, progressively covering the surface of the particles and filling the pore-space. The outward growth rate is defined to be different from that parallel to the surface. The growth of the product leads to an uneven growth front around the particles, similar to simulations C and D shown earlier. A schematic of this mechanism is shown in Fig. 7. The product is assumed have a constant and uniform density of 2.0 g/cm$^3$.

The schematic is only representative and, unlike simulations C and D in Section 2.2, each nuclei is not simulated explicitly here. It is assumed that the nuclei are small enough to consider a uniform unevenness of the growing products over the surface. The covered fraction of the particle surface, $f$, at time $t$, is calculated using the Avrami equation in two dimensions as shown in Eq. (8). Here we use this equation to model the growth of the two-dimensional circular projection of the nuclei on the surface of the alite particles. As the nucleation can be considered to be random and unbiased over the two dimensions of the surface of the particles, the Avrami equation is valid here (see Section 2.1).

$$f = 1 - \exp(-k_1 \cdot t^n) \tag{8}$$

In this equation $k_1$ is the rate constant in the direction parallel to the surface. For the case of randomly distributed nuclei on the surface of the particles ($n=2$ or 3, see Eq. (2)), $k_1$ can be written as:

$$k_1 = \pi G_1^2 \left( N_0 + \frac{I_A}{3} \right) \tag{9}$$

where $N_0$ is the initial number of nuclei per unit area of the surface of the particles, $I_A$ is the rate of nucleation per unit area and $G_1$ is the rate of growth of the nuclei parallel to the surface. In most cases, one of $N_0$ or $I_A$ is assumed to be 0. Since it is assumed that the product grows outwards at a uniform rate $G_2$, the age of the product at a distance r from the centre of the particle, with an original radius $r_0$ can be written as:

$$t_r = \left( t - \frac{(r - r_0)}{G_2} \right) \tag{10}$$

The fraction of the area $f_a$ filled at a distance $r$ from the centre of the particle can then be written as:

$$f_a = 1 - \exp\left( -k_1 \cdot \frac{r_0^2}{r^2} \cdot \left( t - \frac{(r - r_0)}{G_2} \right)^n \right) \tag{11}$$

It was, however, found that the above equation cannot be accurately implemented on μic due to certain numerical limitations[2]

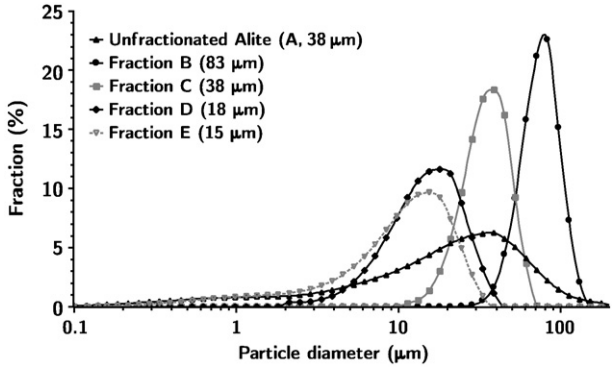


**Fig. 5.** Particle size distributions of different fractions of alite.

[2] In μic, and in the vector approach in general, in the case of overlaps between particles, any point in the microstructure is assumed to be occupied by the particle that arrived there first and cannot be transferred to another particle at a later stage. The partial filling of space being implemented using a progressive change in the density of the product and the rate of outward growth being the same for all particles, only the product growing on the particle which is closest to any point in the microstructure can continue to fill a location since it would be already "allocated" to the closest particle. Due to multiplication of the filling rate by $r_0^2/r^2$, the rate of conversion is significantly slowed down at points where $r >> r_0$ with respect to the sphere closest to them, significantly affecting the shape of the kinetics for systems with smaller particles. This is only a numerical limitation of the chosen implementation of the vector approach since in reality this point could be filled by product coming from a particle that, although a little farther away from this point, has a larger radius, leading to a higher $r_0^2/r^2$.

**Table 3**
The mode diameter, surface-volume mean diameter, presence of fines, 10th 50th and 90th percentile diameters, Blaine and BET surface adsorption fineness of the alite fractions used in this study [18].

| Name | $D_{mode}$ (μm) | $D_{s-vmd}$ (μm) | Has fines | $D_{v10}$ (μm) | $D_{v50}$ (μm) | $D_{v90}$ (μm) | Blaine ($m^2$/kg) | BET ($m^2$/kg) |
|---|---|---|---|---|---|---|---|---|
| *A* | 38.5 | 3.47 | Yes | 1.7 | 20.0 | 59.3 | 190.5 | 597.7 |
| *B* | 82.6 | 71.0 | No | 47.5 | 69.5 | 95.7 | 61.0 | 376.8 |
| *C* | 38.5 | 32.2 | No | 20.4 | 32.4 | 47.3 | 121.2 | 1033.7 |
| *D* | 17.9 | 11.9 | No | 6.3 | 13.8 | 24.5 | 239.3 | 1537.7 |
| *E* | 15.4 | 4.17 | Yes | 2.0 | 10.3 | 20.3 | 305.9 | N.A. |

and it was necessary to assume that the fraction of area covered at any point only depends on how long the product has been present at that location. $f_a$ can now be written as:

$$f_a = 1 - \exp\left(-k_1 \cdot \left(t - \frac{(r - r_0)}{G_2}\right)^n\right) \quad (12)$$

The total amount of product around a grain, $m_i$, at time $t$ can be calculated as:

$$m_i = \int_{r_0}^{r_0 + k_2 \cdot t} 4 \cdot \pi \cdot r^2 \cdot f_a \cdot dr \quad (13)$$

However, due to impingement with the product from other particles only a fraction of the outer surface of the product, $f_{free}$, is available for growth at any moment. This parameter depends on the distance from the original boundary of the particle and is calculated explicitly in μic. The actual amount of products around the grain at time, $t$, can therefore be written as:

$$m_i = \int_{r_0}^{r_0 + G_2 \cdot t} 4 \cdot \pi \cdot r^2 \cdot \left(1 - \exp\left(-k_1 \cdot \left(t - \frac{(r - r_0)}{G_2}\right)^n\right)\right) \cdot f_{free} \cdot dr \quad (14)$$

### 3.1.1. Fit parameters and results

Eq. (14), which has three independent parameters $k_1$, $G_2$ and $n$, was input as a reaction kinetics plugin to μic and was solved numerically to calculate the amount of product around each grain at any moment in time. Since nucleation and growth are demand based mechanisms, the amount of product that can form determines the advancement of the reaction. The results from the simulations are shown in Fig. 8 along with the experimental results for the corresponding powders. The parameters used in the simulations are listed in Table 5. In the table, the parameter $k_1$ has been replaced by $t_{1/2}$, the time at which half the surface of the particles is covered, as shown in Eq. (15).

$$t_{1/2} = \left(\frac{-\ln(0.5)}{k_1}\right)^{(1/n)} \quad (15)$$

The amount of reaction at the start of the acceleration period ($\alpha_0$) was subtracted from the experimental degrees of hydration to account for not simulating the dissolution and induction periods.

In the simulations, the parameters were adjusted to obtain curves close to the experimentally measured ones by manual trial and error. The trials were stopped when it was considered that there was a fair comparison with the experimental results. The position of the peak was found to depend on $t_{1/2}$ and the rate of heat evolution depends on $G_2$. The parameter $n$ was fixed at the same value for all simulations. Better fits were obtained when $n$ was fixed at 3 than when it was fixed at 2. This value of n corresponds to a progressive formation of new nuclei on the surface of alite particles, at least during the first few hours.

A wide variation in the vertical growth rates, $G_2$, was observed indicating that the rate of hydration does not scale well with the specific surface area of the powder. More importantly, it was found that, for all fractions simulated, the heat evolution after the peak continued to be significantly higher than the experimentally observed values. This is because the volume of product, which is consistent with the nucleation and growth of a uniformly dense C–S–H, at the peak was insufficient for significant impingement between growing particles which would lead to a deceleration in the hydration rate. As was demonstrated in simulation D in Section 2.2, although the overlap of nuclei growing on the same particle can stop the acceleration, only a physical barrier to the outward growth of the nuclei, such as impingement with nuclei from other particles, can lead to a deceleration.

This can be seen in Fig. 9, which shows a slice of the simulated microstructure of sample A-38 μm at the peak of heat evolution. The white hydrate rims in the figure indicate the outermost extent of the uneven product surface. This is not surprising since the degree of hydration at peak is between only 6.5% and 14% for the fractions presented in this paper. These results show that a nucleation and growth process on the surface of the particles, and an outward growth rate that corresponds to the experimentally measured heat evolutions alone cannot explain the post-peak deceleration.

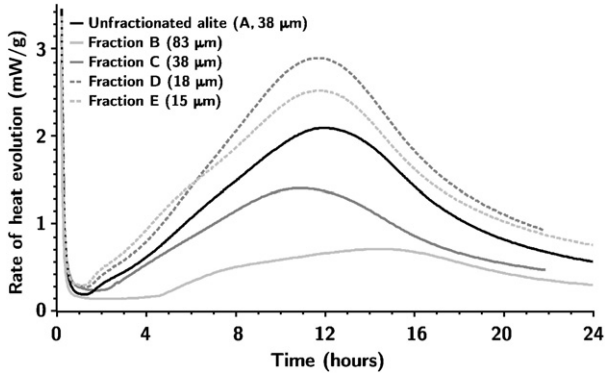


**Fig. 6.** Measured rates of heat evolution for the fractions.

**Table 4**
Number of alite particles and size of computational volume in simulations.

| Fraction | *A*-38 μm | *B*-3 μm | *C*-38 μm | *D*-18 μm | *E*-15 μm |
|---|---|---|---|---|---|
| No. of particles | 2034071 | 241 | 244 | 2173 | 805725 |
| Size (μm) | 100 | 400 | 175 | 100 | 75 |

## 3.2. Existence of a diffusion controlled regime

### 3.2.1. Simulations with a diffusion controlled mechanism

It is often argued that the slow diffusion of ions through the layers of hydrates depositing over the alite particles leads to the deceleration of the rate of reaction [5–7]. In this section we examine this scenario with another set of simulations to study the parameters obtained when a diffusion controlled regime is used to reproduce the measured heat evolution after the peak. As in the previous case, the C–S–H is assumed to grow on the surface of the alite particles in these simulations, while the CH is assumed to form new particles in the pores. The size of the computational volumes and the number of alite particles is the same as in the previous section (see Table 4).

In these simulations, the accelerating part of hydration was simulated using a decomposition of the Avrami equation to the level

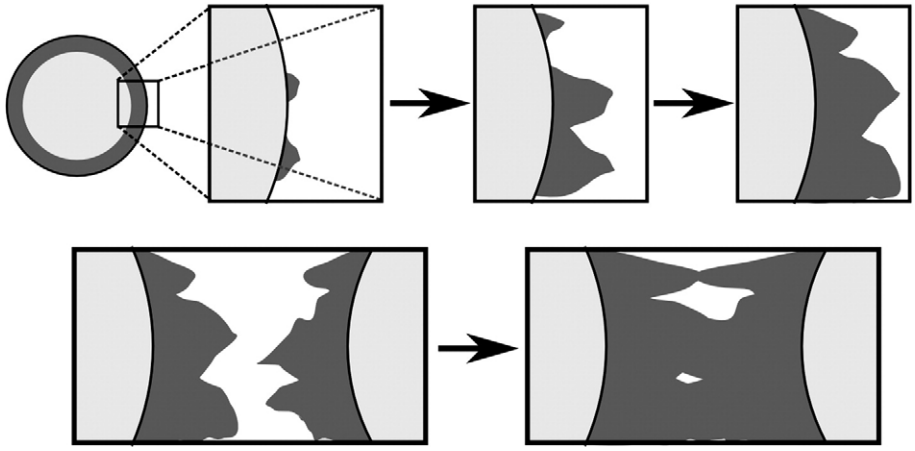

**Fig. 7.** Schematic of the nucleation and growth mechanism with different parallel and outwards growth rates for a single particle (top) and between particles (bottom).

of individual particles with the assumption that the rate of hydration of a particle is proportional the surface area of the reactant, as shown in Eq. (16).

$$\frac{dr_{\text{in}}}{dt} = -k_1 \cdot n \cdot t^{n-1} \cdot e^{-k_1 t^n} \tag{16}$$

Although the Avrami equation does not represent the mechanisms active in alite hydration, here it used only to reproduce the shape of the acceleration and the thickness of product layers during the first few hours of hydration. The more mechanistically accurate Eq. (14) was not used as it leads to an uneven outer surface of the particles, complicating the diffusion calculations. Eq. (17) was used to simulate the diffusion controlled process.

$$\frac{dr_{\text{in}}}{dt} = \frac{-k_{\text{diff}}}{r_{\text{in}}^2 \cdot \left(\frac{1}{r_{\text{in}}} - \frac{1}{r_{\text{out}}}\right)} \tag{17}$$

In this equation, $r_{\text{in}}$ is the radius of the reactant part of the particle and $r_{\text{out}}$ is the outer radius of the product around the particle. The rate constants are combined into the composite parameter $k_{\text{diff}}$, which is proportional to the diffusion coefficient of the reactive species

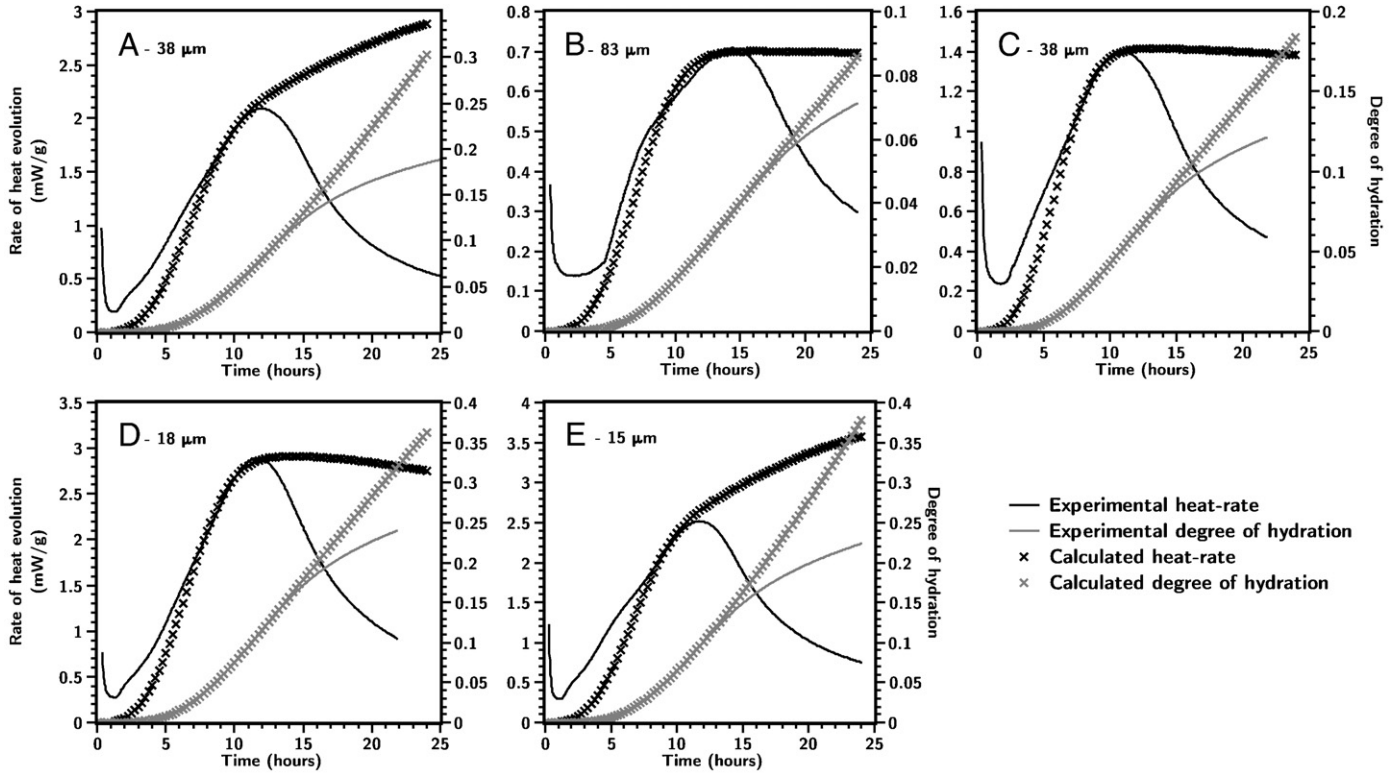


**Fig. 8.** Comparison between simulations and experimental results of heat-evolution rates and degrees of hydration from simulations using the classical definition of nucleation and growth simulations.

**Table 5**
Parameters used in uniform density nucleation and growth simulations.

| Fraction | *A*-38 μm | *B*-83 μm | *C*-38 μm | *D*-18 μm | *E*-15 μm |
|---|---|---|---|---|---|
| $t_{1/2}$(h) | 6.5 | 6.9 | 5.8 | 6.4 | 6.3 |
| $n$ | 3.0 | 3.0 | 3.0 | 3.0 | 3.0 |
| $G_2$(μm/h) | 0.0044 | 0.0315 | 0.0290 | 0.0215 | 0.0058 |
| $\alpha_0$(%) | 3.6 | 2.5 | 2.1 | 2.5 | 4.7 |

through the material. The rate is inversely proportional to the resistance to flow offered by the layer of hydrates around the particles. As it is in spherical coordinates, this equation assumes perfectly radial flows and isotropic diffusion coefficients. The consumption of reactant is also assumed to be uniform over the surface of the particle. In the simulation, the rate is corrected for the reduction of the surface of hydrates in direct contact with water, due to impingement from neighbouring particles.

Eq. (16) was fit to the accelerating part of the evolution such that the calculated rate of hydration fits closely the measured values up to as close to the peak as possible. The mechanism is assumed to switch to diffusion control when the reaction rate predicted by Eq. (17) is lower than that from Eq. (16). This switch is allowed to occur at different moments independently for each particle and can happen only in one direction. The parameter $k_{diff}$ in Eq. (17) was then varied to fit the decelerating part of the curve.

The simulated fits and the experimental curves are shown in Fig. 10. The parameters obtained from the fits are listed in Table 6. In some of the fits, the deceleration obtained was slower than that observed in the experiments.

The diffusion coefficients varied over an order of magnitude, indicating that a large variation in the transport properties of C–S–H has to be assumed in order to explain the deceleration by a diffusion controlled mechanism. This is because the hydrate layer thickness at which diffusion becomes the controlling mechanism is different for different particle size distributions. The minimum, maximum and average thickness of the hydrate layer at the peak ($h_{p,min}$, $h_{p,max}$ and $h_{p,mean}$ respectively) are listed in Table 6. Since the switch to a diffusion controlled mechanism can occur at different moments in time for each particle, the values listed are at the time when the overall rate of reaction for the whole system reduces.

Since no experimental evidence of any difference in C–S–H characteristics between different PSDs was seen by microscopy or other characterization techniques [18], such a large change in the transport properties of C–S–H is unlikely. The resistance to diffusion of ions through the layer of hydrates cannot therefore explain the deceleration in stage 4 of hydration. However, this does not preclude that diffusion processes may be important in the later stages of hydration.

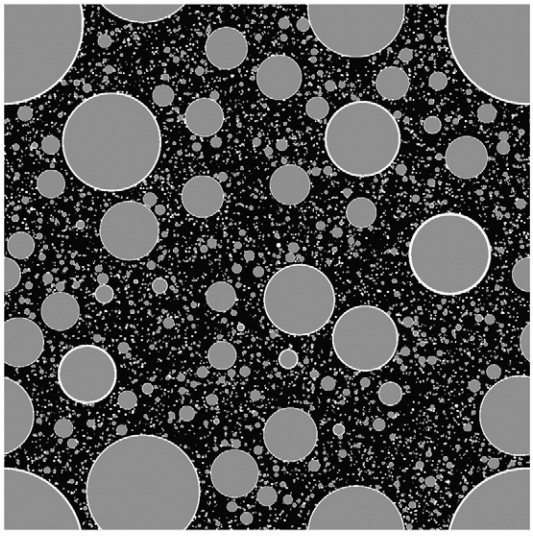

**Fig. 9.** A slice from the simulation of the unfractionated alite (38 μm) at 10 h from simulations using the classical definition of nucleation and growth. The pores are shown in black, alite in dark-grey and the outer boundaries of the hydrates are shown in white.

### 3.3. C–S–H densification with reaction

It has been shown in the previous sections that the values of diffusion coefficients of C–S–H were inconsistent from one alite fraction to another if the deceleration in stage 4 of hydration is assumed to be controlled by the diffusion of ions through the layers of hydrates on the alite particles. It was also shown that due to insufficient impingement between hydrates the nucleation and growth of C–S–H having a density in the currently accepted ranges on the surface of alite particles is not able to reproduce the deceleration. In this section, a slight modification to the nucleation and growth theory is proposed to induce sufficient impingement between the hydrates so that the decelerations simulated follow the trends observed experimentally.

While the kinetics used in these simulations are similar to those in Section 3.1, the bulk density of the product formed or its packing fraction is assumed to increase with hydration. It is assumed that the first product formed has a low packing fraction or bulk density and that this bulk density increases with the advancement of the reaction. The higher volume of this low-density product leads to an earlier impingement between hydrates originating from different particles.

In this study, the rate of hydration is assumed to be controlled by a nucleation and growth mechanism, the main aspects of which are as follows:

The surface of the particles is only partially covered by product, and the availability of product surface controls the growth of product,
Fresh outer product has a low packing fraction,
C–S–H grows uniformly over its exposed outer surface, and
The rate of increase of packing fraction of C–S–H is assumed to decrease linearly with density.

A schematic of this mechanism is shown in Fig. 11. Unlike the previous cases, to simplify the calculations, in these simulations both the CH and C–S–H are assumed to grow on the cement particles. The CH produced is accommodated with the inner product. This was done as, due to the lower bulk density used, the C–S–H produced rapidly fills most of the space, making it difficult to allocate space for the creation and growth of CH particles. The size of the computational volumes and the number of alite particles is the same as that listed in Table 4 earlier.

The amount of material around a particle at any moment in time can be calculated in a way similar to Eq. (14) as follows:

$$m_i = \int_{r_0}^{r_0 + G_2 \cdot t} 4 \cdot \pi \cdot r^2 \cdot \left(1 - \exp\left(-k_1 \cdot \left(t - \frac{(r - r_0)}{G_2}\right)^n\right)\right) \cdot f_{free} \cdot \frac{\rho(r)}{\rho_o} \cdot dr \tag{18}$$

The above relation includes a variable density, $\rho(r)$, which depends on the distance from the centre of the alite particle. This density is the bulk density of C–S–H with a chemical composition equivalent to $C_{1.7}SH_4$, not including any unbound water. It is assumed that the rate of change of density varies linearly with the instantaneous density as follows:

$$\frac{d\rho}{dt} = k_{den} \cdot \frac{\rho_{max} - \rho}{\rho_{max} - \rho_{min}} \tag{19}$$

In the above equation, $\rho_{min}$ and $\rho_{max}$ are the minimum and maximum possible densities of the product respectively and $k_{den}$ is a

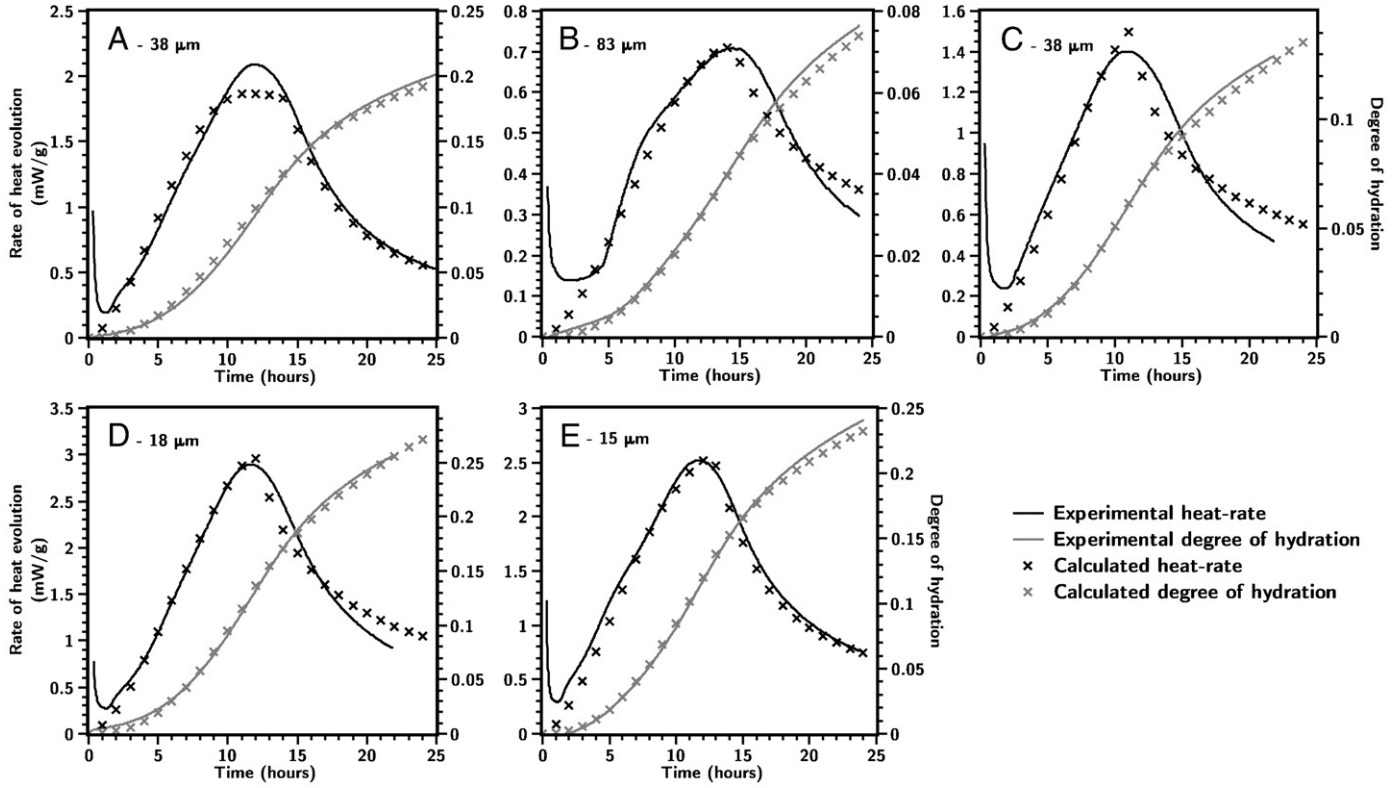


**Fig. 10.** Comparison between simulations and experimental results of heat-evolution rates and degrees of hydration using the diffusion control mechanism.

rate constant. Integrating with time t, for the range 0 to $t_r$, the age of the product (see Eq. (10)) and rearranging we get:

$$\rho = \rho_{max} - (\rho_{max} - \rho_{min}) \cdot \exp\left(\frac{-k_{den} \cdot t_r}{\rho_{max} - \rho_{min}}\right) \quad (20)$$

The above relations are not necessarily exact and only demonstrate that the modelled mechanisms can explain the observed hydration mechanism.

### 3.3.1. Fit parameters and results

Eqs. (18) and (20), which have six independent parameters namely $k_1$, $G_2$, $n$, $k_{den}$, $\rho_{min}$ and $\rho_{max}$, were solved numerically in a plugin in μic to calculate the amount of product around the grains at any moment in time. As in Section 3.1, the rates of reaction were calculated from the demand generated from the nucleation and growth process described above. The value of $\rho_{max}$ was set to 2.0 g/cm$^3$ for all simulations, this was also assumed to be the density of the inner product. The value of $n$ was again fixed at 3.0. The other four parameters could be varied to control the three main features of the curves, namely the time of peak, the height of the peak and the rate of deceleration.

Once again the parameter $k_1$ was replaced by $t_{1/2}$ (see Eq. (15)). Since the density of the inner product was fixed at the highest possible density of the product, the actual average density of the product at all times is higher than $\rho_{min}$. The fit parameters were obtained by manual trial and error and the trials were stopped when fair agreements were obtained.

The position of the peak was observed to depend on $t_{1/2}$ and $G_2$, while $G_2$ and $k_{den}$ were observed to have a combined effect on the rate of hydration. The parameters $G_2$, $k_{den}$ and $\rho_{min}$ have a combined effect on the heat evolution at peak and also the rate of heat evolution after the peak. As can be seen in Fig. 12, good fits were obtained for all particle size distributions for a large part of the first 24 h. The parameters used are listed in Table 7. Fig. 13 shows the change in the curves with a variation in different parameters for fraction *D*-38 μm. In the curve marked "alternative parameters" in Fig. 13, the value of $G_2$ was doubled and the other parameters were freely modified to obtain a curve similar to that for the fraction $D = 38$ μm (see Table 7), showing that a significantly different set of parameters can be used to obtain a similar curve with only a slight difference in shape, partially explaining the spread in the parameters.

It was found that the required values of the initial density of outer C–S–H were significantly lower than those reported in literature [23,24]. The values of the density listed here represent the bulk density of C–S–H, with a molar mass 227.2 approximated by the formula $C_{1.7}SH_4$ not including the weight of any unbound water that may be present in the pores. Based on the values reported by Jennings [25], a density of 0.2 would be equivalent to 1.19 g/cm$^3$ of bulk wet density, if the weight of the unbound water is included.

The variation in the parameter $G_2$ is quite large. As shown in Fig. 14, it was found to be lower for finer particle size distributions that have a higher number of particles per unit volume and therefore a smaller distance between neighbours. This trend is an obvious implication of the model used as the peak in the rate of hydration occurs at around the same time for all fractions. In order to have sufficient impingement between hydrates from neighbouring particles to lead to a deceleration, a lower rate of perpendicular growth is required in fractions with lower average distance between particles.

**Table 6**
Details of Avrami equation and diffusion equation simulations.

| Fraction | *A*-38 μm | *B*-83 μm | *C*-38 μm | *D*-8 μm | *E*-15 μm |
|---|---|---|---|---|---|
| $K_1$ ($h^{-n}$) | $1.25\times10^{-4}$ | $5.60\times10^{-4}$ | $6.70\times10^{-4}$ | $4.50\times10^{-4}$ | $1.54\times10^{-4}$ |
| $n$ | 2.6 | 2.6 | 2.6 | 2.6 | 2.6 |
| $k_{diff}$ (μm$^2$/h) | $3.20\times10^{-3}$ | $3.80\times10^{-2}$ | $2.40\times10^{-2}$ | $1.60\times10^{-2}$ | $3.20\times10^{-3}$ |
| $t_0$ (h) | 0.0 | 0.0 | 0.0 | 0.0 | 0.0 |
| $\alpha_0$ (%) | 2.3 | 2.0 | 1.3 | 0.9 | 3.0 |
| $h_{p,min}$ (μm) | 0.02 | 0.68 | 0.48 | 0.08 | 0.0006 |
| $h_{p,max}$(μm) | 0.16 | 0.71 | 0.51 | 0.43 | 0.14 |
| $h_{p,mean}$ (μm) | 0.10 | 0.69 | 0.49 | 0.40 | 0.11 |

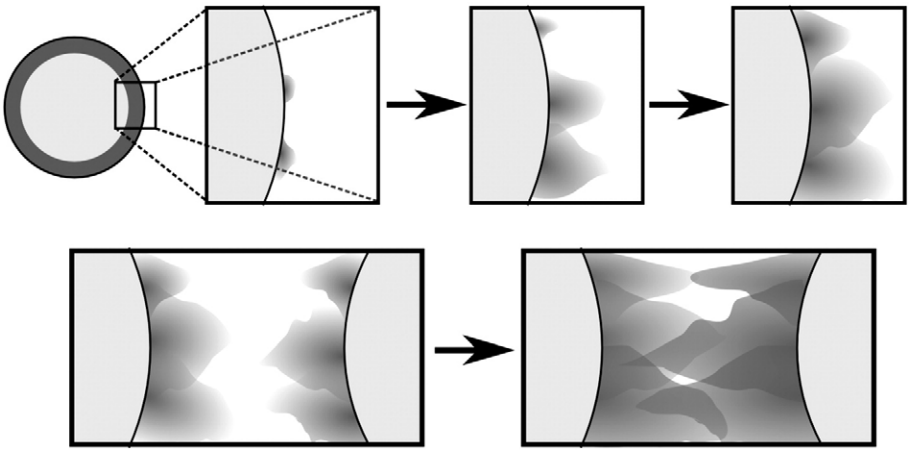

**Fig. 11.** Schematic of the nucleation and growth mechanism with different parallel and outwards growth rates and densification of the product for a single particle (top) and between particles (bottom).

Fig. 15 shows a slice of the simulated fraction A — 38 μm at the peak, with the reach of the hydrates marked in white. It can be seen in the figure, that the low density product has filled a significant portion of the microstructure at the peak, explaining the deceleration after the peak observed in the simulations.

## 4. Discussion

The results in this study suggest the presence of a loosely-packed product filling a large part of the microstructure from quite an early age. That such a microstructure is rarely seen in micrographs of cement and alite paste could be attributed to the drying involved in the process of sample preparation required for microscopy. However, a loose, low-density structure of C–S–H, growing as a loose packing of fibres or sheets can still be observed in many micrographs (e.g. Fig. 16) [26–28]. Recent SEM images (see Fig. 17) have also shown the presence of a loosely dispersed C–S–H throughout the microstructure around the peak of hydration [29].

The presence of C–S–H with variable density has been proposed earlier to explain surface area measurements by nitrogen adsorption [8,24]. It was also shown that the specific surface area of C–S–H reduces with time, indicating an increase in density of the product. A progressive densification of the product was also proposed much earlier by Powers [30]. Since all experimental techniques measure

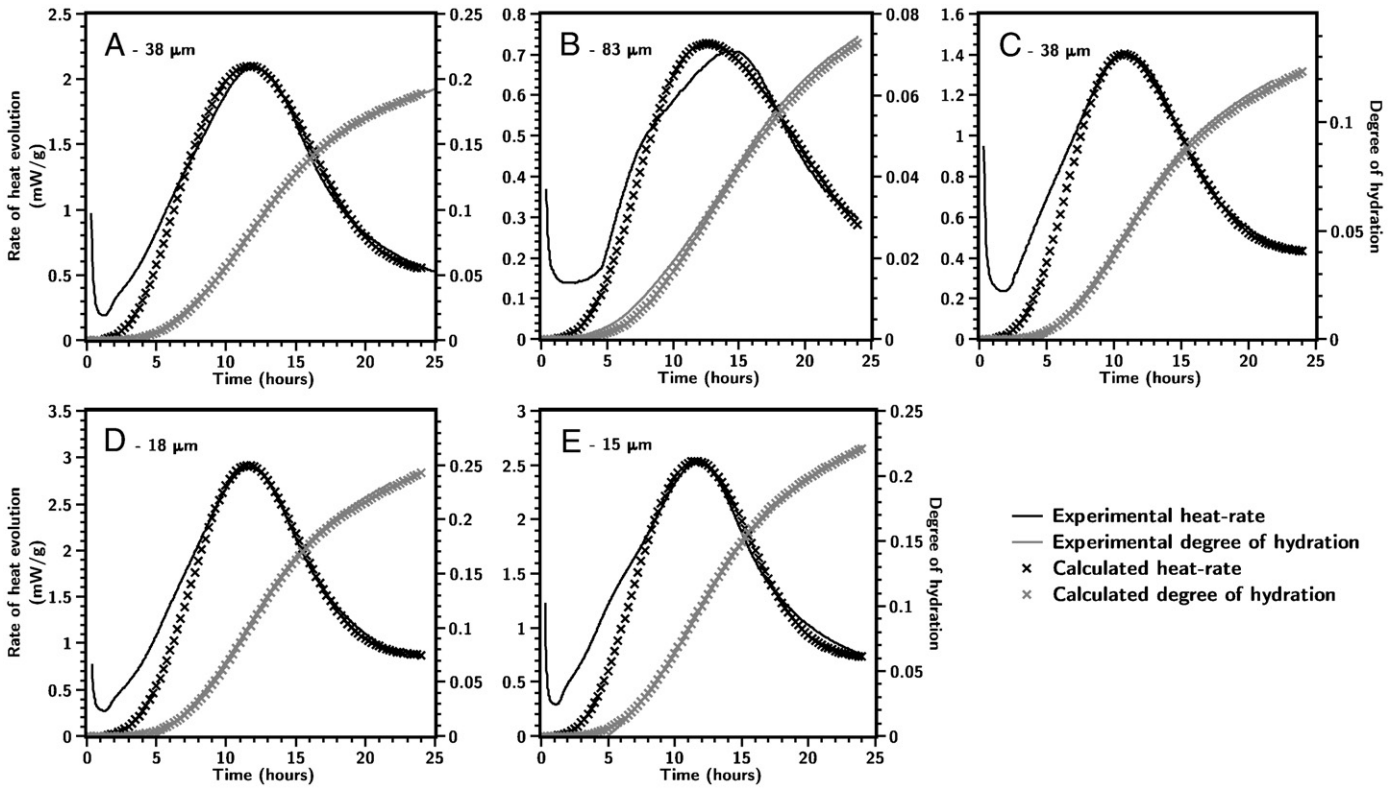


**Fig. 12.** Comparison between simulations and experimental results of heat-evolution rates and degrees of hydration for simulations with variable density of product.

**Table 7**
Parameters used in variable density nucleation and growth simulations.

| Fraction | *A*-38 μm | *B*-83 μm | *C*-38 μm | *D*-18 μm | *E*-15 μm | *D*-18 μm alternative |
|---|---|---|---|---|---|---|
| $t_{1/2}$ (h) | 4.9 | 6.9 | 6.2 | 7.4 | 5.2 | 8.8 |
| $n$ | 3.0 | 3.0 | 3.0 | 3.0 | 3.0 | 3.0 |
| $G_2$ (μm/h) | 0.032 | 1.10 | 0.77 | 0.35 | 0.039 | 0.70 |
| $k_{den}$ (g/cm$^3$/h) | 0.007 | 0.0020 | 0.0056 | 0.012 | 0.01 | 0.0115 |
| $\rho_{min}$ (g/cm$^3$) | 0.22 | 0.100 | 0.11 | 0.185 | 0.222 | 0.145 |
| $\alpha_0$ (%) | 3.2 | 2.20 | 2.30 | 3.15 | 4.8 | – |

only the average bulk values and most measurements are only possible after a few days of hydration, a much higher variation could exist at an early age at the micro-level. In Quasi-elastic neutron scattering and NMR relaxation measurements of pore-sizes, which do not entail sample-drying, indicate that a larger than expected fraction of the water at this stage is close to the surface of hydration products [31–33]. The presence of a loosely-packed product can also explain the early setting of paste even at low degree of hydration, when just a small amount of product can lead to the transformation of the paste from a viscous liquid to a visco-elastic solid.

The low packing coupled with the high outward growth rates indicate that C–S–H grows as a fine mesh throughout a large portion of the microstructure within a few hours of hydration and the variation of the growth rate with inter-particle spacing appears to indicate the opportunistic nature of this growth depending on the availability of space. While it is expected that a similar change in the growth rate would be observed for systems with different water to cement ratios, further study is needed to understand the combined effect of the lower surface available for nucleation and the higher volume available for growth per unit volume of paste in systems with higher water to cement ratios.

At present there is no conclusive evidence of the presence of a loosely-packed product. It is not claimed that the hypothesis presented is a literal representation of the hydration mechanism and the spread in the fitting parameters indicates that refinements may be needed to the inputs and to the precise model used. However, the study points towards an important possibility for microstructural development, which requires further investigation. It is important to note that the simulations provide strong evidence that the nucleation and growth of C–S–H, with densities in the range currently accepted, cannot explain the observed alite hydration rates beyond the peak.

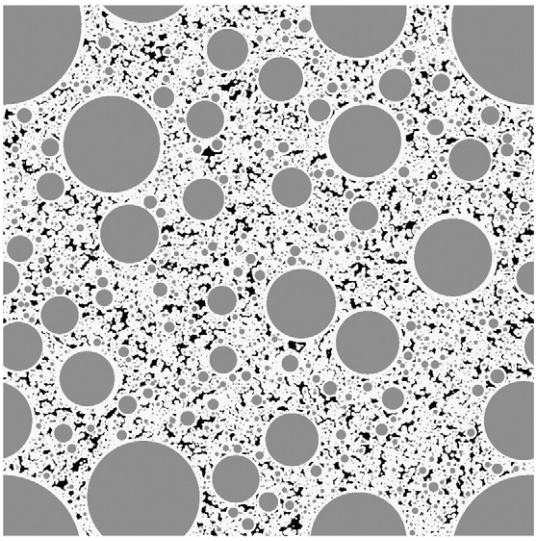

**Fig. 15.** A slice from simulation on the unfractionated alite (*A*-38 μm) with densifying C–S–H at 10 h. Pores are shown in black, anhydrous grains in dark grey and the outer boundaries of the hydrates are shown in white.

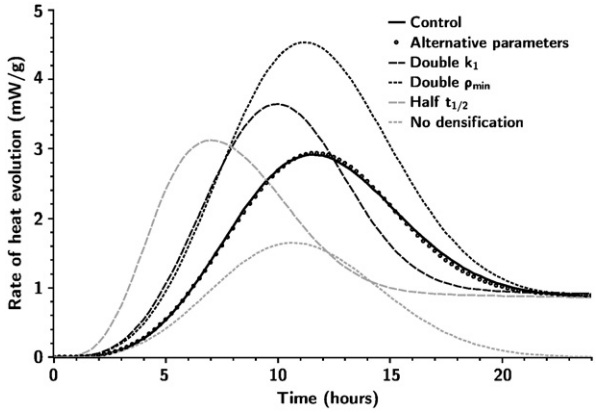


**Fig. 13.** Dependence of simulated heat evolution on parameters for fraction *D*-18 μm. The alternative parameters curve shows the reproduction of a similar evolution using a different set of parameters where $G_2$ was fixed at double the value used and other parameters were freely modified.

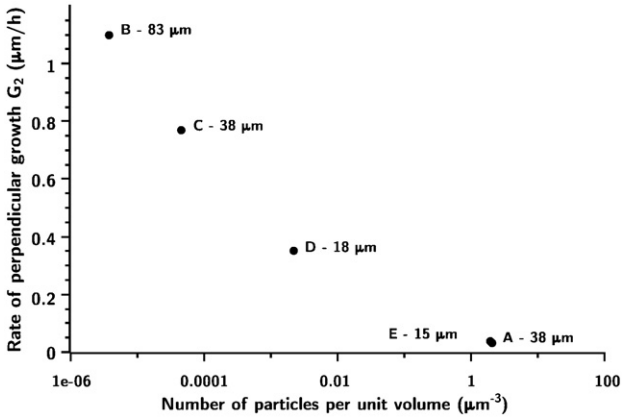


**Fig. 14.** Variation of $G_2$ with the number of particles per unit volume in the simulations.

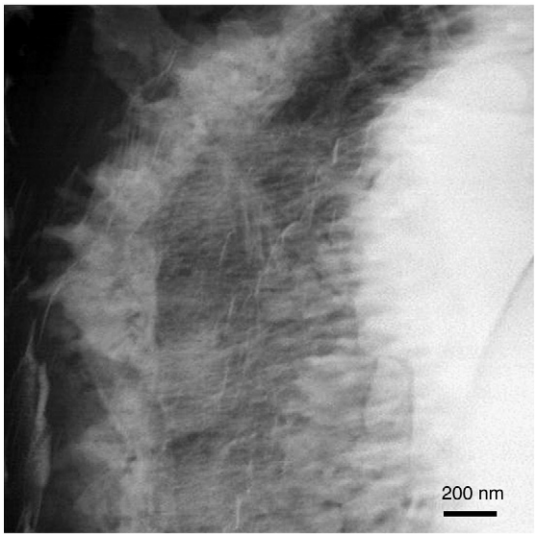


**Fig. 16.** TEM image of OPC at 12 h of hydration showing a relatively loosely-packed C–S–H (from Mathur 2007 [28]).

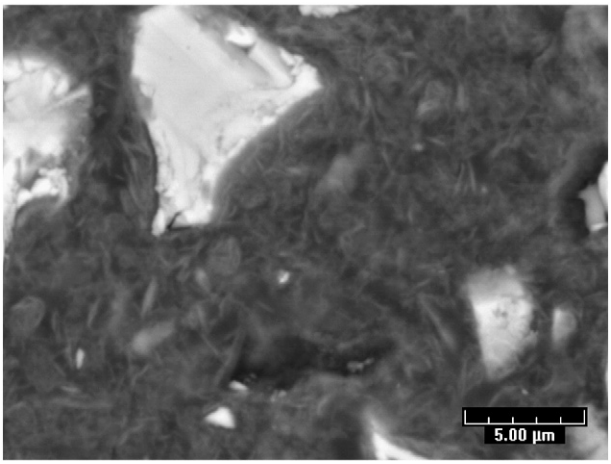


**Fig. 17.** SEM micrograph by Juilland [29] showing a loosely-packed C–S–H distributed throughout the microstructure in an alite sample close to its peak of hydration. The alite was mixed with water in a high-shear mixer at 995 rpm for 2 min and then after being left undisturbed for 13 min, it was mixed again for 1 min at 995 rpm.

Neither can a diffusion controlled mechanism explain the decelerating part of hydration, unless it is accepted that hydrates have widely varying diffusion properties.

## 5. Conclusions

In this paper, the hydration kinetics of alite were investigated using the modelling platform µic. First it was demonstrated that while the Avrami and BN equations can be used to predict the rates of reactions in systems similar to those used for the derivation of these equations, they are not suitable for alite or cement.

Two different nucleation and growth mechanisms and a diffusion controlled mechanism were implemented in simulations on alite powders with particle size distributions similar to those used experimentally. It was shown that the nucleation and growth of C–S–H, with currently accepted values of its density, cannot explain the deceleration observed during the hydration of alite. Furthermore, in order to explain the deceleration using a diffusion controlled regime, drastic changes in the transport properties of C–S–H from different alite particles would have to be assumed. In contrast the reaction kinetics for most of the first 24 h of hydration can be well reproduced using a nucleation and growth mechanism where a loosely-packed C–S–H is assumed to form and fill a large fraction of the pore-space by the peak of hydration. Although the hypothesis of a loosely-packed fast space filling C–S–H needs further investigation, it appears to capture the important features of the rate of heat development during alite hydration.

This work also demonstrates the versatility of µic to simulate a wide range of phenomenon in three dimensions and shows how microstructural models can be used to study hydration mechanisms.

## Acknowledgement

The authors gratefully acknowledge the financial support from the Swiss National Science Foundation project number 200020-112063/1. The authors thank Dr. Mercedes Costoya for providing the experimental results. We would also like to thank Patrick Juilland for letting us use his SEM images. Latest information about the development status of µic, user documentations and freely downloadable source codes and executables of µic and its graphical user interface, including all the plugins and modules used in this publication can be found on the µic web page [17].

## References

[1] N. Tenoutasse, A. De Donder, Silicates Industriels 35 (1970) 301–307.
[2] A. Bezjak, I. Jelenic, On the determination of rate constants for hydration processes in cement pastes, Cement and Concrete Research 10 (1980) 553–563.
[3] S. Garrault, A. Nonat, Hydrated layer formation on tricalcium and dicalcium silicate surfaces: experimental study and numerical simulations, Langmuir 17 (2001) 8131–8138.
[4] J.J. Thomas, A new approach to modeling the nucleation and growth kinetics of tricalcium silicate hydration, Journal of the American Ceramic Society 90 (2007) 3282–3288.
[5] R. Kondo, S. Ueda, Kinetics of hydration of cements, Proceedings of the 5th international symposium on chemistry of cement, Tokyo, 1968, pp. 203–248.
[6] E.M. Gartner, J.F. Young, D.A. Damidot, I. Jawed, Hydration of portland cement, Structure and Performance of Cements, 2nd ed., Spon Press, London, 2002.
[7] S. Garrault, T. Behr, A. Nonat, Formation of the C–S–H layer during early hydration of tricalcium silicate grains with different sizes, Journal of Physical Chemistry 110 (2006) 270–275.
[8] P.D. Tennis, H.M. Jennings, A model for two types of calcium silicate hydrate in the microstructure of Portland cement pastes, Cement and Concrete Research 30 (2000) 855–863.
[9] W.A. Johnson, R.F. Mehl, Reaction kinetics in processes of nucleation and growth, Transactions of the Americal Institute of Mining and Metallurgy 135 (1939) 416–458.
[10] M. Avrami, Kinetics of phase change. I, Journal of Chemical Physics 7 (1939) 1103–1112.
[11] A. Kolmogorov, Statistical theory of crystallization of metals (in Russian), Akademiia nauk SSSR Izvestiia Seriia khimicheskaia (Bulletin of the Academy of Sciences of the USSR. Division of chemical sciences) 3 (1937) 355–359.
[12] J.B. Austin, R.L. Rickett, Kinetics of the decomposition of austenite at constant temperature, Transactions of the American Institute of Mining, Metallurgical, and Petroleum Engineers 135 (1939) 396–443.
[13] J.J. Thomas, H.M. Jennings, Effects of D2O and mixing on the early hydration kinetics of tricalcium silicate, Chemistry of Materials 11 (1999) 1907–1914.
[14] P.W. Brown, J. Pommersheim, G. Frohnsdroff, A kinetics model for the hydration of tricalcium silicate, Cement and Concrete Research 15 (1985) 35–41.
[15] J.W. Cahn, The kinetics of grain boundary nucleated reactions, Acta Metallurgica 4 (1956) 449–459.
[16] S. Bishnoi, K.L. Scrivener, µic: a new platform for modelling the hydration of cements, Cement and Concrete Research 39 (2009) 266–274.
[17] S. Bishnoi, Webpage of µic the modelling platform, www.micthemodel.org.
[18] M. Costoya, Kinetics and microstructural investigation on the hydration of tricalcium silicate, Doctoral Thesis, École Polytechnique Fédérale de Lausanne, Switzerland, 2008.
[19] T. Knudsen, Modelling hydration of portland cement: the effect of particle size distribution, Proceedings of the Engineering Foundation Conference, 1983.
[20] H.F.W. Taylor, Cement Chemistry, Thomas Telford, 1997.
[21] H.M. Jennings, L.J. Parrott, Microstructural analysis of hardened alite paste, Part II: Microscopy and reaction products, Journal of Materials Science 21 (1986) 4053–4059.
[22] P. Navi, C. Pignat, Simulation of cement hydration and the connectivity of the capillary pore space, Advanced Cement Based Materials 4 (1996) 58–67.
[23] T.C. Powers, Structure and physical properties of hardened Portland cement paste, Journal of American Ceramic Society 41 (1958) 1–6.
[24] H.M. Jennings, A model for the microstructure of calcium silicate hydrate in cement paste, Cement and Concrete Research 30 (2000) 101–116.
[25] H.M. Jennings, Colloid model of C–S–H and implications to the problem of creep and shrinkage, Materials and Structures 37 (2004) 59–70.
[26] A. Grudemo, An electronographic study of the morphology and crystrallization properties of calcium silicate hydrates, Procedings of the Swedish Cement and Concrete Institute, vol. 26, Royal Institute of Technology, Stockholm, 1955, p. 103.
[27] I.G. Richardson, The nature of C–S–H in hardened cements, Cement and Concrete Research 29 (1999) 1131–1147.
[28] P.C. Mathur, Study of cementitious materials using transmission electron microscopy, Doctoral Thesis, École Polytechnique Fédérale de Lausanne, 2007.
[29] P. Juilland, Personal Communication.
[30] T.C. Powers, Physical properties of cement paste, Proceedings of the Fourth International Symposium on Chemistry of Cement, Washington, USA, 1960, pp. 577–613.
[31] W.P. Halperin, Jyh-Yuar Jehngb, Yi-Qiao Song, Application of spin–spin relaxation to measurement of surface area and pore size distributions in a hydrating cement paste, Magnetic Resonance Imaging 12 (1994) 169–173.
[32] E. Fratini, S.-H. Chen, P. Baglioni, M.-C. Bellissent-Funel, Quasi-elastic neutron scattering study of translational dynamics of hydration water in tricalcium silicate, Journal of Physical Chemistry B 106 (2002) 158–166.
[33] P.J. McDonald, J. Mitchell, M. Mulheron, L. Monteilhet, J.-P. Korb, Two-dimensional correlation relaxation studies of cement pastes, Magnetic Resonance Imaging 25 (2007) 470–473.